Transfer of polarized infrared radiation in optically anisotropic media: application to horizontally oriented ice crystals

Y. Takano and K. N. Liou

Center for Atmospheric and Remote Sounding Studies, Department of Meteorology, University of Utah, Salt Lake City, Utah 84112

Received July 15, 1992; revised manuscript received November 30, 1992; accepted December 8, 1992

We have developed a theory for the computation of the polarization of infrared radiation in optically anisotropic media, with specific application to horizontally oriented ice crystals that frequently occur in cirrus clouds. Both emission and scattering contributions are accounted for in the basic formulation concerning the transfer of thermal radiation in anisotropic media. The symmetry relations of the phase matrix elements for horizontally oriented ice crystals, which are required in the infrared polarization formulations, are presented for the first time to our knowledge. Phase matrix elements for horizontally oriented hexagonal ice crystals are computed by a geometric ray-tracing technique. Radiance and linear-polarization patterns at a 10-μm wavelength that are emergent from cirrus clouds that contain plates and columns oriented in two-dimensional space are presented and discussed in physical terms. Downward polarization emergent from the cloud base is negative, while upward polarization emergent from the cloud top has a positive maximum value near the limb directions. These polarization configurations differ distinctly from the configurations of polarization emergent from ice clouds that contain randomly oriented ice crystals in three-dimensional space. Given these results, it appears feasible to infer the orientation characteristics of ice crystals in cirrus clouds with the use of infrared polarization measurements either above or below the cloud.

1. INTRODUCTION

The apparent infrared signatures of aircraft often depend on the infrared transmission and radiance properties of cirrus clouds. In our previous papers[1,2] we developed methodologies for the computation of infrared radiances and linear polarization for randomly oriented hexagonal ice crystals. However, ice crystals in cirrus clouds often are oriented with their maximum dimensions horizontal and are referred to as horizontally oriented ice crystals.[3] Although the transfer of solar irradiance and the associated polarization configuration in cirrus clouds that contain horizontally oriented ice crystals have been formulated and numerically studied by Takano and Liou,[4,5] radiance and polarization patterns associated with thermal infrared radiation, in which emission plays an important role, have not been investigated.

In this paper we develop a theory and a numerical scheme for the computation of infrared polarization patterns in optically anisotropic media, with application to horizontally oriented ice crystals. In Section 2 we present the basic formulation concerning the transfer of thermal radiation, including polarization in anisotropic media. We describe a procedure for calculating anisotropic polarization for thermal radiation emitted from horizontally oriented ice crystals. We also present a numerical scheme based on the adding principle for radiative transfer. In Section 3 we discuss the symmetry relations with respect to the phase matrix for horizontally oriented ice crystals. In Section 4 we present phase matrix elements for plates and columns oriented in two-dimensional (2D) space for visible and infrared wavelengths computed with a geometric ray-tracing technique, and we display and discuss infrared radiance and linear-polarization patterns at cirrus cloud boundaries. We present our conclusions in Section 5.

2. TRANSFER OF POLARIZED INFRARED RADIATION IN OPTICALLY ANISOTROPIC MEDIA

A. Radiative-Transfer Equation

Following the well-known principle (see, e.g., Ref. 6), the differential change in the Stokes vector, $\mathbf{dI}$, after traveling a thickness, dz/μ, in the direction of the propagation can be expressed in the form

$$\begin{aligned}\mathbf{dI}(z,\mu,\phi) = &-\beta_e(\mu)\mathbf{I}(z,\mu,\phi)dz/\mu \\ &+\frac{1}{4\pi}\int_0^{2\pi}\int_{-1}^{1}\beta_s(\mu')\mathbf{Z}(\mu,\mu',\phi,\phi')\mathbf{I}(z,\mu',\phi')d\mu'd\phi' \\ &+\beta_a(\mu)B_\lambda(T)\mathbf{I}_e, \qquad (1)\end{aligned}$$

where μ is the cosine of the zenith angle, θ; z is the vertical distance; ϕ is the azimuthal angle; β_e, β_s, and β_a are the extinction, the scattering, and the absorption coefficients, respectively; $\mathbf{Z}$ is the phase matrix with respect to the local meridian plane; $B_\lambda(T)$ is the Planck radiance of temperature T at a wavelength λ; and $\mathbf{I}_e$ is the emitted Stokes vector. Generally, β_e, β_s, and β_a are functions of ϕ and z as well as of μ. In the present study, however, the dependence of these coefficients on ϕ and z is neglected on the assumption that ice crystals are oriented randomly in a horizontal plane and that they are distributed uniformly in the vertical direction. The first term on the right-hand side of Eq. (1) denotes an attenuation along the path. The

0740-3232/93/061243-14$06.00

second and the third terms denote increments that are due to multiple scattering and to thermal emission, respectively. Next we introduce the differential normal optical depth, $d\tilde{\tau}$, in the form

$$d\tilde{\tau} = -\tilde{\beta}_e dz, \tag{2}$$

where $\tilde{\beta}_e$ is the extinction coefficient in the vertical direction, $\beta_e(\mu = 1)$. When Eq. (1) is divided by $d\tilde{\tau}$, we obtain the radiative-transfer equation in the form

$$\mu \frac{d\mathbf{I}(\tilde{\tau}, \mu, \phi)}{d\tilde{\tau}} = k(\mu)\mathbf{I}(\tilde{\tau}, \mu, \phi) - \mathbf{J}(\tilde{\tau}, \mu, \phi), \tag{3}$$

where $k(\mu)$ is the extinction coefficient normalized by the vertical extinction coefficient:

$$k(\mu) = \beta_e(\mu)/\tilde{\beta}_e. \tag{4}$$

The source function, $\mathbf{J}$, is given by

$$\mathbf{J}(\tilde{\tau}, \mu, \phi) = \frac{1}{4\pi}\int_0^{2\pi}\int_{-1}^{1} \tilde{\omega}^*(\mu')\mathbf{Z}(\mu, \mu', \phi, \phi')\mathbf{I}(\tilde{\tau}, \mu', \phi')d\mu' d\phi' + k(\mu)[1 - \tilde{\omega}(\mu)]B_\lambda(T)\mathbf{I}_e. \tag{5}$$

In Eq. (5), the true single-scattering albedo $\tilde{\omega}$ and the apparent single-scattering albedo $\tilde{\omega}^*$ are given in the forms

$$\tilde{\omega}(\mu) = \beta_s(\mu)/\beta_e(\mu), \tag{6a}$$

$$\tilde{\omega}^*(\mu) = \beta_s(\mu)/\tilde{\beta}_e. \tag{6b}$$

The appearance of the true and the apparent single-scattering albedos in Eq. (5) is due to the fact that multiple scattering is proportional to the scattering cross section in the incident direction, μ', whereas emission is proportional to the absorption cross section in the emergent direction, μ.

The emitted infrared polarized radiation is symmetrical with respect to the azimuthal angle. For this reason we may use only the zeroth Fourier component of the radiance in the discussion of radiative transfer. On averaging the general radiative-transfer equation, Eq. (3), with respect to the azimuthal angle, we can express the transfer equation for polarized infrared radiation in the form

$$\mu \frac{d\mathbf{I}(\tilde{\tau}, \mu)}{d\tilde{\tau}} = k(\mu)\mathbf{I}(\tilde{\tau}, \mu) - \mathbf{J}(\tilde{\tau}, \mu). \tag{7}$$

Here, $\mathbf{I}$ is the 2D Stokes vector, (I, Q). Now the source function, $\mathbf{J}$, can be written in the form

$$\mathbf{J}(\tilde{\tau}, \mu) = \tfrac{1}{2}\int_{-1}^{1} \tilde{\omega}^*(\mu')\hat{\mathbf{Z}}(\mu, \mu')\mathbf{I}(\tilde{\tau}, \mu')d\mu' + k(\mu)[1 - \tilde{\omega}(\mu)]B_\lambda(T)\begin{bmatrix}1\\ Q_e\end{bmatrix}. \tag{8}$$

$\hat{\mathbf{Z}}$ is the 2×2 phase matrix, which will be derived in Section 3. $-\mathbf{Q}_e$ is the linear polarization associated with emission, which is derived in Subsection 2B.

B. Evaluation of the Polarization Term Q_e

To formulate the anisotropic polarization of the emitted radiation, let the major axis of a hexagonal column be the c axis and a pair of prism planes be in the horizontal plane (i.e., a Parry column) as shown in Fig. 1. Consider a light beam emitted from the basal plane in a direction, OE, specified by the zenith angle, θ, and the relative azimuthal angle, $\phi - \phi'$. The angle between direction OE and the normal direction of the basal plane, OX, is denoted σ. The angle between the reference plane with respect to the emitting plane, EOX, and the reference plane with respect to the local meridian plane, EOZ, is denoted δ. To obtain the polarization patterns for thermal emission in the infrared region, we may use a procedure similar to that for emission from calm ocean surfaces at microwave frequencies. A light beam reflected by a flat surface has no elliptical polarization. On the basis of this principle, the fourth Stokes parameter, V, must be 0 for a light beam that is emitted from a flat surface. In other words, a light beam emitted from a flat surface is linearly polarized. The third Stokes parameter, U, is also 0, as a result of the symmetry of emission with respect to the normal of the surface. Therefore the Stokes vector (I_l, I_r, U, V) emitted from a flat surface to a zenith angle θ can be written as $(1 - |r_l(\theta)|^2, 1 - |r_r(\theta)|^2, 0, 0)$, where r_l and r_r are the Fresnel reflection coefficients. In the case of the horizontally oriented ice crystals, the normal direction of each crystal plane does not always coincide with the zenith direction, OZ, as in the case of calm ocean surfaces. Thus the reference plane with respect to the emitting plane, EOX, in Fig. 1, must be converted to the local meridian plane, EOZ, by application of the transform matrix, $\hat{\mathbf{L}}$, to the above Stokes vector. Transformation matrix $\hat{\mathbf{L}}$ can be expressed in the form

$$\hat{\mathbf{L}}(\delta) = \begin{bmatrix} \cos^2\delta & \sin^2\delta & \tfrac{1}{2}\sin 2\delta & 0 \\ \sin^2\delta & \cos^2\delta & -\tfrac{1}{2}\sin 2\delta & 0 \\ -\sin 2\delta & \sin 2\delta & \cos 2\delta & 0 \\ 0 & 0 & 0 & 1 \end{bmatrix}. \tag{9}$$

As a result, the Stokes parameters I_l, I_r, U, and V emitted from a certain crystal plane can be expressed as

$$\begin{aligned} I_l &= \cos^2\delta[1 - |r_l(\sigma)|^2] + \sin^2\delta[1 - |r_r(\sigma)|^2], \\ I_r &= \sin^2\delta[1 - |r_l(\sigma)|^2] + \cos^2\delta[1 - |r_r(\sigma)|^2], \\ U &= \sin 2\delta[|r_l(\sigma)|^2 - |r_r(\sigma)|^2], \\ V &= 0. \end{aligned} \tag{10}$$

Angles σ and δ can be obtained easily from the scattering geometry shown in Fig. 1. The two polarization compo-

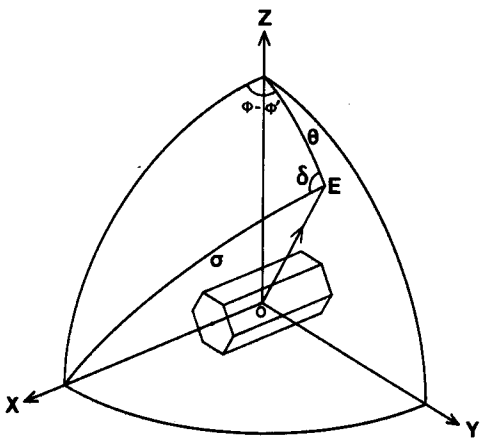

Fig. 1. Emission geometry for Parry columns.

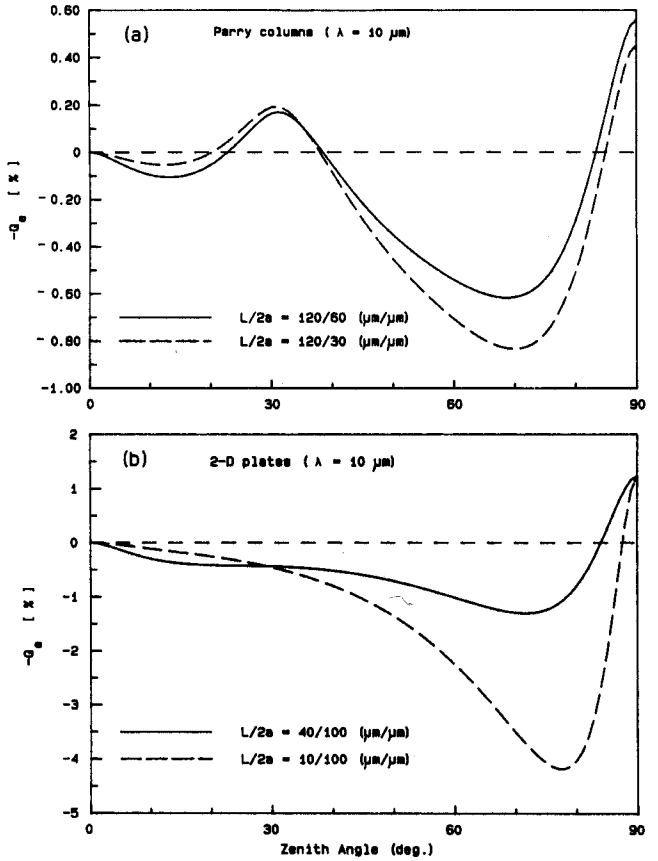

Fig. 2. Degree of linear polarization, $-Q_e$, for thermal radiation emitted from (a) Parry columns and (b) 2D plates.

nents, $\bar{I}_l$ and $\bar{I}_r$, emitted from an ensemble of Parry columns located randomly in a horizontal plane, are equivalent to those for a single fixed Parry column averaged with respect to the relative azimuthal angle, $\phi - \phi'$. We may carry out integration of $I_{l,r}$, weighted by the effective area of each crystal plane with respect to the relative azimuth, to obtain the averaged values in the form

$$\bar{I}_{l,r}(\theta) = \frac{\int_0^{2\pi} \sum_i I_{l,r}{}^i \cos \sigma_i A_i \mathrm{d}(\phi - \phi')}{\int_0^{2\pi} \sum_i \cos \sigma_i A_i \mathrm{d}(\phi - \phi')}, \tag{11}$$

where i is the suffix expressing each crystal plane and A_i is the area of crystal planes. $\bar{U}$ is 0 because δ is an odd function of $\phi - \phi'$.

Figure 2 shows the degree of linear polarization, $-Q_e \equiv -(\bar{I}_l - \bar{I}_r)/(\bar{I}_l + \bar{I}_r)$, of radiation emitted from Parry columns and 2D plates (plate crystals with the short c axis vertical) at a wavelength of 10 μm. The complex refractive index of ice[7] used in this computation is $1.1991 - i0.051$. If ice crystals are oriented randomly, the degree of linear polarization, $-Q_e$, is zero. Negative polarization at $\theta \leq 80°$ and positive polarization at $\theta \gtrsim 80°$ can be interpreted by the relation $r_l \leq r_r$ between the Fresnel reflection coefficients. As shown in Fig. 2(b), the computed values of negative polarization can reach -4% in the case of flat 2D plates. Generally, magnitudes of polarization for 2D plates [Fig. 2(b)] are greater than those for Parry columns [Fig. 2(a)], because the relative area of 2D plates with respect to the vertical is greater than that of Parry columns.

C. Solution of the Radiative Transfer Equation

The adding principle for radiative transfer[8] may be used to evaluate the transfer of polarized infrared radiation in cloud layers. On the basis of successive tracing of the radiation beam, as illustrated in Fig. 3, the upward ($\mathbf{J}_u$) and the downward ($\mathbf{J}_d$) source terms at the interface of the two layers denoted by a and b are given, in the notation of Ref. 5, by

$$\begin{aligned}\mathbf{J}_d &= [\mathbf{1} + \mathbf{R}_a{}^*\mathbf{R}_b + (\mathbf{R}_a{}^*\mathbf{R}_b)^2 + \ldots]\mathbf{J}_a{}^- \\ &\quad + [\mathbf{1} + \mathbf{R}_a{}^*\mathbf{R}_b + (\mathbf{R}_a{}^*\mathbf{R}_b)^2 + \ldots]\mathbf{R}_a{}^*\mathbf{J}_b{}^+ \\ &= (\mathbf{1} + \mathbf{S})(\mathbf{J}_a{}^- + \mathbf{R}_a{}^*\mathbf{J}_b{}^+), \end{aligned} \tag{12}$$

$$\begin{aligned}\mathbf{J}_u &= [\mathbf{1} + \mathbf{R}_b\mathbf{R}_a{}^* + (\mathbf{R}_b\mathbf{R}_a{}^*)^2 + \ldots]\mathbf{J}_b{}^+ \\ &\quad + [\mathbf{1} + \mathbf{R}_b\mathbf{R}_a{}^* + (\mathbf{R}_b\mathbf{R}_a{}^*)^2 + \ldots]\mathbf{R}_b\mathbf{J}_a{}^- \\ &= (\mathbf{1} + \mathbf{S}^*)(\mathbf{J}_b{}^+ + \mathbf{R}_b\mathbf{J}_a{}^-), \end{aligned} \tag{13}$$

where $\mathbf{1}$ is the identity matrix, $\mathbf{R}$ is the reflection matrix, the superscript * denotes quantities associated with radiation from below, and the multiple-reflection terms are defined by

$$\mathbf{S} = \mathbf{R}_a{}^*\mathbf{R}_b(\mathbf{1} - \mathbf{R}_a{}^*\mathbf{R}_b)^{-1}, \tag{14}$$

$$\mathbf{S}^* = \mathbf{R}_b\mathbf{R}_a{}^*(\mathbf{1} - \mathbf{R}_b\mathbf{R}_a{}^*)^{-1}. \tag{15}$$

If we use the upward and the downward source terms at the interface, the upward and the downward source terms at the top and the bottom of the combined layer are given by

$$\mathbf{J}_{ab}{}^+ = \mathbf{J}_a{}^+ + \tilde{\mathbf{T}}_a{}^*\mathbf{J}_u, \tag{16}$$

$$\mathbf{J}_{ab}{}^- = \mathbf{J}_b{}^- + \tilde{\mathbf{T}}_b\mathbf{J}_d, \tag{17}$$

where the total transmission matrix, $\tilde{\mathbf{T}}$, is the sum of the diffuse plus the direct components:

$$\tilde{\mathbf{T}} = \mathbf{T} + \exp(-\tau/\mu). \tag{18}$$

For a homogeneous layer, the reflection matrix and the diffuse-transmission matrix are the same regardless of

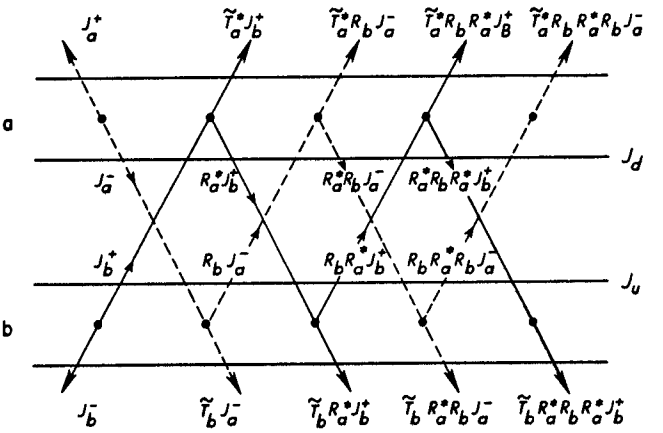

Fig. 3. Geometric configuration of the adding method used to evaluate thermal emission. The dashed and the solid lines represent radiation emitted from layers a and b, respectively.

radiation from below or above. That is, $\mathbf{R}^* = \mathbf{R}$ and $\mathbf{T}^* = \mathbf{T}$. It follows that the multiple-reflection term $\mathbf{S}^* = \mathbf{S}$ in Eqs. (14) and (15).

For a thin layer having an optical thickness $\Delta\tilde{\tau}$, the upward and the downward Stokes vectors, $\mathbf{J}^+$ and $\mathbf{J}^-$, resulting from emission from a gray body in the emergent direction, μ, can be obtained from Eq. (8) as follows:

$$\mathbf{J}^+(\mu) = \mathbf{J}^-(\mu) = k(\mu)[1 - \tilde{\omega}(\mu)]B_\lambda(T)\begin{bmatrix}1\\ Q_e\end{bmatrix}\Delta\tilde{\tau}/\mu. \quad (19)$$

For a thin layer, the reflection and the diffuse-transmission matrices can be computed from the phase matrix in the forms

$$\mathbf{R}(\mu,\mu') = \frac{\tilde{\omega}^*(\mu')\Delta\tilde{\tau}}{4\mu\mu'}\hat{\mathbf{Z}}(\mu,-\mu'), \quad (20a)$$

$$\mathbf{T}(\mu,\mu') = \frac{\tilde{\omega}^*(\mu')\Delta\tilde{\tau}}{4\mu\mu'}\hat{\mathbf{Z}}(\mu,\mu'), \quad (20b)$$

where $\hat{\mathbf{Z}}(\mu,\mu')$ is the azimuthally averaged component of the phase matrix $\mathbf{Z}(\mu,\mu',\phi - \phi')$, which is defined in Section 3. Starting from Eqs. (19) and (20), we repeat the above adding procedure to attain a desired optical depth. Finally, the surface emission can be considered a separate layer, with emission pointing only upward.

3. PHASE MATRIX FOR HORIZONTALLY ORIENTED ICE CRYSTALS

To describe scattering processes, we define the amplitude matrix, $\mathbf{A}$, in the form

$$\begin{bmatrix}E_l\\ E_r\end{bmatrix} = \frac{\exp(-ikR + ikz)}{ikR}\begin{bmatrix}A_2 & A_3\\ A_4 & A_1\end{bmatrix}\begin{bmatrix}E_l^0\\ E_r^0\end{bmatrix}, \quad (21)$$

where $\mathbf{E}^0 = (E_l^0, E_r^0)$ and $\mathbf{E} = (E_l, E_r)$ are the incident and scattered electric vectors, respectively, k is the wave number of the incident light, R is the distance between the scatterers and the observer, z is the distance from the scatterers along the incident direction, and $i = \sqrt{-1}$. The phase matrix $\mathbf{P}$ is defined in the form

$$\begin{bmatrix}I\\ Q\\ U\\ V\end{bmatrix} = \frac{1}{k^2R^2}\begin{bmatrix}P_{11} & P_{12} & P_{13} & P_{14}\\ P_{21} & P_{22} & P_{23} & P_{24}\\ P_{31} & P_{32} & P_{33} & P_{34}\\ P_{41} & P_{42} & P_{43} & P_{44}\end{bmatrix}\begin{bmatrix}I_0\\ Q_0\\ U_0\\ V_0\end{bmatrix}, \quad (22)$$

where (I_0, Q_0, U_0, V_0) and (I, Q, U, V) are the incident and the scattered Stokes vectors, respectively. Generally, if no assumption is made on the scatterers, the phase matrix consists of 16 elements.

To derive the symmetry relations of the phase matrix for horizontally oriented crystals, we consider a pair of horizontally oriented crystals that are mirror images with respect to the principal meridian plane. Let a pair of parallel rays be incident upon the two crystals (either two plates or two columns). A pair of incident points upon the two crystals can be considered, since an arbitrary point on one crystal will always have a symmetrical counterpart on the other crystal. The two incident rays that are reflected and/or refracted are also emergent to the symmetrical directions with respect to the principal meridian plane, i.e., to directions $(\theta_n, \phi_n - \phi')$ and $(\theta_n, \phi' - \phi_n)$, where θ is the zenith angle and $\phi - \phi'$ is the azimuthal angle. The subscript n represents the order of the scattered light rays.[9] The directions of the normals at each incident point upon the two crystals are also symmetrical. The signs of the rotational angles of the coordinate axis at each incident point for a pair of scattered rays are opposite. As a result, the signs of the nondiagonal elements of the 2×2 amplitude matrix, $A^{(n)}$, are also opposite, as is pointed out in Ref. 9. The diagonal elements, $A_1^{(n)}$ and $A_2^{(n)}$, are even functions of $\phi - \phi'$, and the nondiagonal elements, $A_3^{(n)}$ and $A_4^{(n)}$, are odd functions of $\phi - \phi'$ when ice crystals are oriented horizontally. This symmetry relation is expressed symbolically as

$$\mathbf{A}^{(n)} = \begin{bmatrix}A_2^{(n)} & A_3^{(n)}\\ A_4^{(n)} & A_1^{(n)}\end{bmatrix} = \begin{bmatrix}c & s\\ s & c\end{bmatrix}. \quad (23)$$

In this research, the geometric ray-tracing method is used for the computation of the amplitude matrix, $\mathbf{A}^{(n)}$. The geometrical optics is an approximation based on the assumption that light may be thought of as consisting of separate localized rays that travel along a straight-line path. In Fig. 4, I denotes an incident ray, L is the length of the ice crystal, and $2a$ is the width. The ray denoted $n = 0$ is an externally reflected ray. The ray denoted $n = 1$ is a transmitted ray without internal reflections. In the framework of geometrical optics, the amplitude matrix $\mathbf{A}^{(n)}$ for the nth ray can be written in the form

$$\mathbf{A}'^{(n)} = w_n\mathbf{P}_{sn}\mathbf{T}_n\mathbf{P}_n\left[\prod_{k=n-1}^{2}\mathbf{R}_k\mathbf{P}_k\right]\mathbf{T}_1\mathbf{P}_1, \quad (24a)$$

$$\mathbf{A}^{(n)} = \mathbf{P}_{tn}\mathbf{A}'^{(n)}\mathbf{P}_{-en}, \quad (24b)$$

where w_n is a weight concerned with the flux conservation and $\mathbf{T}_n$ and $\mathbf{R}_n$ are the transmission and the reflection matrices, respectively, which are expressed by

$$\mathbf{T}_n = \begin{bmatrix}t_l^n & 0\\ 0 & t_r^n\end{bmatrix}, \quad \mathbf{R}_n = \begin{bmatrix}r_l^n & 0\\ 0 & r_r^n\end{bmatrix}, \quad (25)$$

where t_l^n and t_r^n are the Fresnel transmission coefficients and r_l^n and r_r^n are the Fresnel reflection coefficients. The matrix $\mathbf{P}_n$ denotes the rotation of coordinate system by an angle ϕ_n, which is given in the form

$$\mathbf{P}_n = \begin{bmatrix}\cos\phi_n & -\sin\phi_n\\ \sin\phi_n & \cos\phi_n\end{bmatrix}. \quad (26)$$

Next we consider the symmetry relations with respect to the phase matrix that transforms the incident Stokes parameters (I_0, Q_0, U_0, V_0) to the scattered Stokes parameters (I, Q, U, V). The phase matrix $\mathbf{G}^{(n)}$ for the geometric rays is expressed explicitly by the elements of the amplitude matrix $\mathbf{A}^{(n)}$ in the form[10]

$$\mathbf{G} = \begin{bmatrix} (M_2 + M_3 + M_4 + M_1)/2 & (M_2 - M_3 + M_4 - M_1)/2 & S_{23} + S_{41} & -D_{23} - D_{41} \\ (M_2 + M_3 - M_4 - M_1)/2 & (M_2 - M_3 - M_4 + M_1)/2 & S_{23} - S_{41} & -D_{23} + D_{41} \\ S_{24} + S_{31} & S_{24} - S_{31} & S_{21} + S_{34} & -D_{21} + D_{34} \\ D_{24} + D_{31} & D_{24} - D_{31} & D_{21} + D_{34} & S_{21} - S_{34} \end{bmatrix}, \quad (27)$$

where M_k, S_{kl}, and D_{kl} are given by

$$\begin{aligned} M_k &= A_k A_k^*, \\ S_{kl} &= S_{lk} = 1/2(A_l A_k^* + A_k A_l^*), \\ -D_{kl} &= D_{lk} = i/2(A_l A_k^* - A_k A_l^*), \\ &\qquad \text{for } k, l = 1\text{–}4. \end{aligned} \quad (28)$$

For simplicity, the superscript n is omitted in the above equations. The phase matrix elements, $\hat{P}_{kl}$, are calculated by adding the contributions from the geometric rays, $G_{kl}^{(n)}$, and the Fraunhofer diffracted ray,[11] G_D, in the form

$$\hat{P}_{kl} = (1 - f_D)\sum_n G_{kl}^{(n)} + \delta_{kl} f_D G_D. \quad (29)$$

In this equation, δ_{kl} is the Kronecker delta and f_D is the fraction of diffracted rays, which is given in the form

$$f_D = \frac{1}{2\tilde{\omega}(1 - f_\delta)}, \quad (30)$$

where f_δ is the δ function transmission at the 0° scattering angle, which is discussed in Ref. 4. From the symmetry relation of the amplitude matrix denoted in Eq. (23), the elements inside the boxes in Eq. (27) are odd functions of $\phi - \phi'$, and the other elements are even functions of $\phi - \phi'$. Since G_D is an even function of $\phi - \phi'$, $\hat{\mathbf{P}}$ has the same symmetry relation as Eq. (27). To evaluate diffraction by a nonspherical ice crystal, we use the Babinet principle: the distribution of light intensity diffracted by a particle is identical to that diffracted by an aperture with shape and size identical to the geometric shadow of the particle. The projections of the eight vertices of a hexagonal crystal on the plane normal to an incident direction are denoted by B_i' in Fig. 5, where Θ and Φ are the scattering and the azimuthal angles, respectively, of the diffracted light beam. The diffraction integral over the geometric shadow area defined by B_i' can be performed easily.

As shown in Ref. 4, the phase matrix elements P_{kl} for plate crystals with the c axis vertical (2D plates) are given by

$$P_{kl}(\theta, \theta', \phi - \phi') = \frac{3}{\pi}\int_0^{\pi/3} \hat{P}_{kl}(\theta, \theta', \phi - \phi'; \beta)\mathrm{d}\beta, \quad k, l = 1\text{–}4, \quad (31)$$

where β is the angle expressing the rotation of the crystal around the c axis, as shown in Fig. 6(a). If the symmetry relation denoted in Eq. (27) is used, Eq. (31) can be written as

$$P_{kl}(\theta, \theta', |\phi - \phi'|) = \frac{6}{\pi}\int_0^{\pi/6} \hat{P}_{kl}(\theta, \theta', \phi - \phi'; \beta)\mathrm{d}\beta, \quad (32)$$

$$P_{kl}(\theta, \theta', |\phi - \phi'|) = \frac{6}{\pi}\int_0^{\pi/6} \mathrm{sgn}(\phi - \phi')\hat{P}_{kl}(\theta, \theta', \phi - \phi'; \beta)\mathrm{d}\beta \quad (33)$$

for the elements outside and inside the boxes in Eq. (27), respectively. Here $\mathrm{sgn}(x) = x/|x|$. Also according to Ref. 4, the phase matrix elements P_{kl} for columnar crystals with both the c axis and a pair of prism planes horizontal (Parry columns) are given by

$$P_{kl}(\theta, \theta', \phi - \phi') = \frac{3}{\pi^2}\int_{-\pi/2}^{\pi/2}\mathrm{d}\gamma\int_0^{\pi/3} \hat{P}_{kl}(\theta, \theta', \phi - \phi'; \gamma, \beta) \times \delta(\beta - \beta^*)\mathrm{d}\beta, \quad k, l = 1\text{–}4, \quad (34)$$

where $\delta = 1$ when $\beta = \beta^*$ and $\delta = 0$ otherwise, β^* is an angle that is defined in Ref. 4, and γ is the angle denoting the orientation of the c axis in the horizontal plane, which is illustrated in Fig. 6(b). If the symmetry relation given in Eq. (27) is used, Eq. (34) can be written as

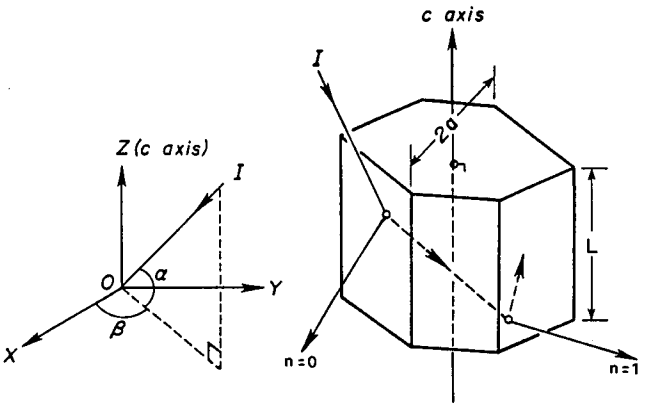

Fig. 4. Geometry of a light ray in an ice crystal: α is the angle between the incident ray and the c axis defined in the diagram, β is the angle of rotation about the axis, I denotes the incident ray, L is the length of the ice crystal, and $2a$ is the width.

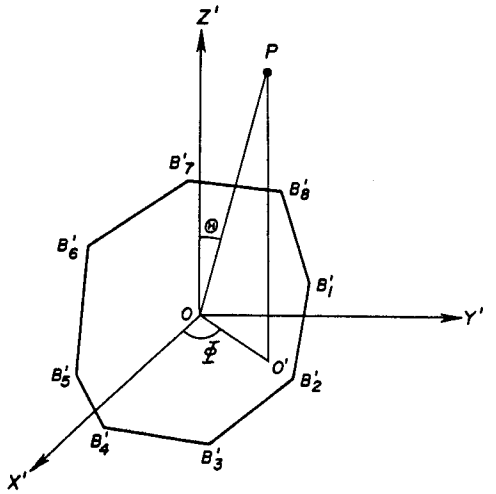

Fig. 5. Geometry for Fraunhofer diffraction at an arbitrary point, P. The projections of the eight vertices of a hexagonal crystal on the plane normal to an oblique incident ray are denoted by $B_i'(i = 1\text{–}8)$. Θ and Φ are the scattering and the azimuthal angles, respectively, of the diffracted light beam.

Angles i_1 and i_2, are given by

$$\cos i_1 = \frac{-\mu + \mu' \cos\Theta}{\pm(1 - \cos^2\Theta)^{1/2}(1 - \mu'^2)^{1/2}}, \tag{39}$$

$$\cos i_2 = \frac{-\mu' + \mu \cos\Theta}{\pm(1 - \cos^2\Theta)^{1/2}(1 - \mu^2)^{1/2}}, \tag{40}$$

where Θ is the scattering angle, which can be written in the form

$$\cos\Theta = \mu\mu' + (1 - \mu^2)^{1/2}(1 - \mu'^2)^{1/2}\cos(\phi - \phi'). \tag{41}$$

In Eqs. (39) and (40), the plus is to be taken when $\pi < \phi - \phi' < 2\pi$ and the minus when $0 < \phi - \phi' < \pi$. Using the 16 nonzero phase matrix elements of $\mathbf{P}$, we can write $\mathbf{Z}$ explicitly as

$$\mathbf{Z} = \begin{bmatrix} P_{11} & P_{12}C' + P_{13}S' & -P_{12}S' + P_{13}C' & P_{14} \\ P_{12}C - P_{31}S & P_{22}CC' - P_{32}SC' + P_{23}CS' - P_{33}SS' & -P_{22}CS' + P_{32}SS' + P_{23}CC' - P_{33}SC' & P_{24}C - P_{34}S \\ P_{21}S + P_{31}C & P_{22}SC' + P_{32}CC' + P_{23}SS' + P_{33}CS' & -P_{22}SS' - P_{32}CS' + P_{23}SC' + P_{33}CC' & P_{24}S + P_{34}C \\ P_{41} & P_{42}C' + P_{43}S' & -P_{42}S' + P_{43}C' & P_{44} \end{bmatrix}. \tag{42}$$

$$P_{kl}(\theta,\theta',|\phi - \phi'|) = \frac{6}{\pi^2}\int_0^{\pi/2} d\gamma \int_0^{\pi/3} \hat{P}_{kl}(\theta,\theta',\phi - \phi';\gamma,\beta) \times \delta(\beta - \beta^*)d\beta, \tag{35}$$

$$P_{kl}(\theta,\theta',|\phi - \phi'|) = \frac{6}{\pi^2}\int_0^{\pi/2} d\gamma \int_0^{\pi/3} \mathrm{sgn}(\phi - \phi') \times \hat{P}_{kl}(\theta,\theta',\phi - \phi';\gamma,\beta)\delta(\beta - \beta^*)d\beta, \tag{36}$$

for the elements outside and inside the boxes in Eq. (27), respectively.

As is well known, the phase matrix defined with respect to the local meridian plane, $\mathbf{Z}(\theta,\theta',\phi - \phi')$, can be obtained by premultiplication and postmultiplication of $\mathbf{P}$ with $\mathbf{L}(\pi - i_2)$ and $\mathbf{L}(-i_1)$ in the form[5]

$$\mathbf{Z}(\theta,\theta',\phi - \phi') = \mathbf{L}(\pi - i_2)\mathbf{P}\mathbf{L}(-i_1), \tag{37}$$

where $\mathbf{L}(\pi - \alpha)$ is the rotation matrix of angle $\pi - \alpha$, which is expressed in the form

$$\mathbf{L}(\pi - \alpha) = \mathbf{L}(-\alpha) = \begin{bmatrix} 1 & 0 & 0 & 0 \\ 0 & \cos 2\alpha & -\sin 2\alpha & 0 \\ 0 & \sin 2\alpha & \cos 2\alpha & 0 \\ 0 & 0 & 0 & 1 \end{bmatrix}. \tag{38}$$

For simplicity, the following abbreviations are used:

$$S' = \sin(2i_1), \quad C' = \cos(2i_1), \quad S = \sin(2i_2), \quad C = \cos(2i_2). \tag{43}$$

Since i_1 and i_2 are odd functions of $\phi - \phi'$, as shown in Eqs. (39) and (40), S' and S are odd functions of $\phi - \phi'$ and C' and C are even functions of $\phi - \phi'$. If we use the symmetry relation with respect to $\mathbf{P}$ denoted in Eq. (27), the elements of $\mathbf{Z}$ inside the boxes in Eq. (42) are odd functions of $\phi - \phi'$ and the other elements are even functions of $\phi - \phi'$. Only the azimuthally averaged term (i.e., the zeroth Fourier component) contributes to the infrared radiative transfer. Hence the matrix elements inside the boxes in Eq. (42) are zero. The Stokes vector of radiation emitted from horizontally oriented ice crystals is $(I, Q, 0, 0)$, which is defined in Section 2. Furthermore, the surface is assumed to emit unpolarized isotropic radiation. Thus, for the computations of the infrared radiances and linear polarization, only the following 2×2 matrix is required:

$$\hat{\mathbf{Z}} = \begin{bmatrix} P_{11} & P_{12}C' + P_{13}S' \\ P_{21}C - P_{31}S & P_{22}CC' - P_{32}SC' + P_{23}CS' - P_{33}SS' \end{bmatrix}. \tag{44}$$

The azimuthally averaged component of $\hat{\mathbf{Z}}$ is used for infrared radiative-transfer computations by means of Eqs. (20a) and (20b).

The symmetry relations of the phase matrix for randomly oriented nonspherical particles in three-

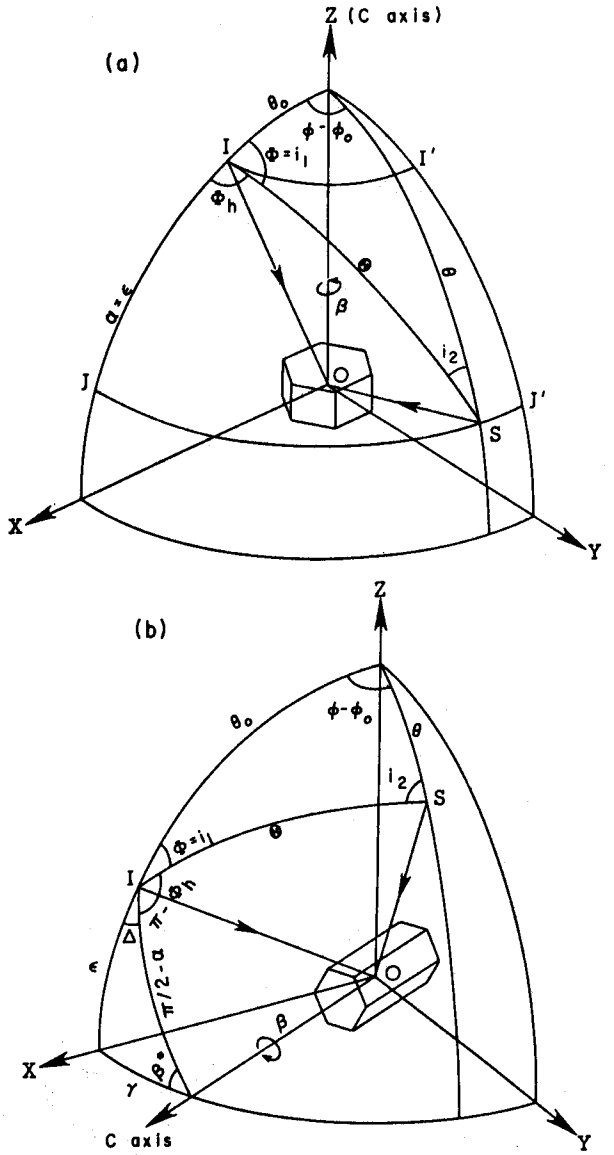

Fig. 6. Scattering geometries for horizontally oriented (a) plate crystals and (b) columnar crystals. *IO* and *SO* denote the incident and the scattered directions, respectively. Other symbols are explained in the text.

dimensional (3D) space have been derived by Hovenier.[12] In the following, we discuss the symmetry relations of the phase matrix for horizontally oriented ice crystals. Consider Eqs. (39)–(41). If the signs of μ, μ', ϕ, and ϕ' are changed simultaneously, Θ, $i_1(=\Phi)$, and i_2 will remain the same. For this reason, $\mathbf{Z}$ as defined in Eq. (37) will also remain unchanged. Thus the symmetry relation C developed by Hovenier,

$$\mathbf{Z}(-\mu, -\mu', \phi' - \phi) = \mathbf{Z}(\mu, \mu', \phi - \phi'), \qquad (C),$$

is valid for horizontally oriented ice crystals. The symmetry relation expressed in Eq. (42) is referred to as the symmetry relation D and can be rewritten as follows:

$$\mathbf{Z}(\mu, \mu', \phi' - \phi) = \mathbf{M}\mathbf{Z}(\mu, \mu', \phi - \phi')\mathbf{M}, \qquad (D),$$

where $\mathbf{M}$ is the mirror matrix,[13] which is defined by

$$\mathbf{M} = \begin{bmatrix} 1 & 0 & 0 & 0 \\ 0 & 1 & 0 & 0 \\ 0 & 0 & -1 & 0 \\ 0 & 0 & 0 & -1 \end{bmatrix}. \qquad (45)$$

However, other symmetry relations (A, B, E, and F) derived by Hovenier, which are valid in a slab of randomly oriented particles with a plane of symmetry, are not appli-

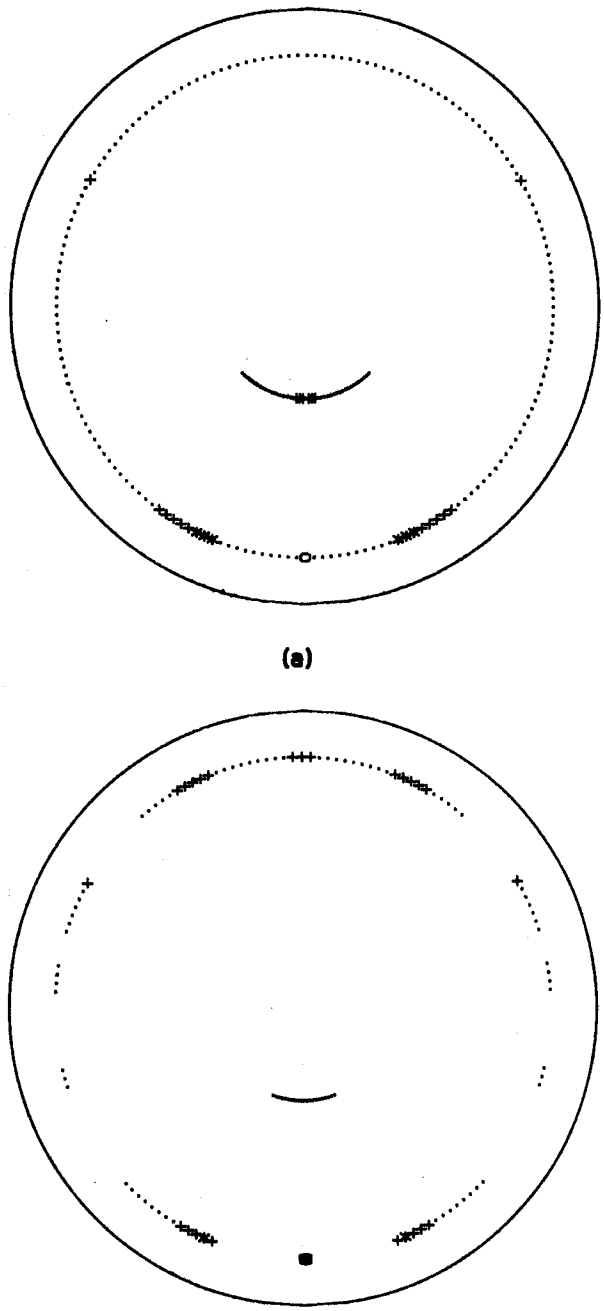

Fig. 7. Phase function, P_{11}, for 2D plates with aspect ratio $L/2a$ of 0.4 at $\lambda = 0.55$ μm (a) above the horizon and (b) below the horizon. The diffracted-light component is excluded so that geometrical-optics ray patterns can be clearly understood. The small circle in (a) indicates the incident solar direction whose zenith angle θ' is 77°. The symbols ·, +, *, and ■ denote 0, 1, 2, and 3, respectively, in units of $[\log_{10} P_{11}]$, where [] denotes the integral part.

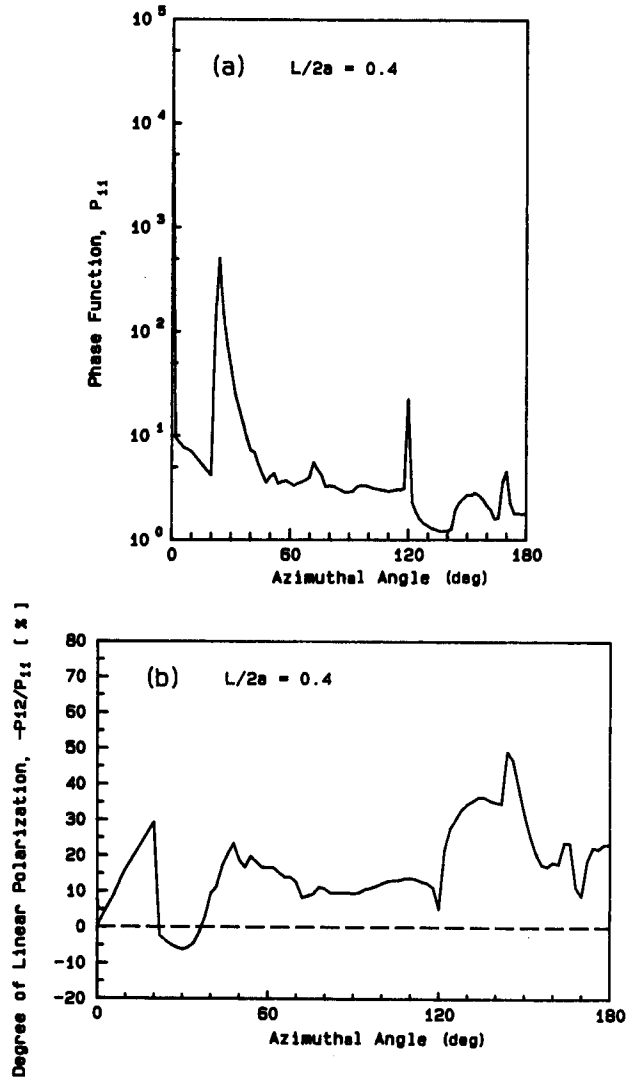

Fig. 8. (a) Phase function P_{11} corresponding to Fig. 7 and (b) degree of linear polarization, $-P_{12}/P_{11}$, along the parhelic circle as a function of the azimuthal angle, $\phi - \phi'$.

cable to the case of horizontally oriented ice crystals, because Z_{13}, Z_{14}, Z_{23}, Z_{24}, Z_{41}, Z_{42}, Z_{31}, and Z_{32} are generally nonzero elements.

4. RESULTS AND DISCUSSION

In order to evaluate infrared polarization from cirrus clouds consisting of horizontally oriented hexagonal ice crystals, we must first compute the single-scattering properties for these ice crystals. In our previous research[4] we developed a geometric ray-tracing program for calculating the phase function P_{11}. However, we must have other phase matrix elements, P_{12}, P_{21}, P_{22}, P_{31}, P_{32}, P_{13}, P_{23}, and P_{33}, as indicated by Eq. (44), to evaluate linear polarization in multiple scattering. To compute these elements, we must take into account the rotation of coordinate systems in relation to the incident plane.[14] According to Ref. 9, the effect of phase shift can be neglected. Furthermore, since we are concerned with infrared wavelengths in which significant absorption within ice crystals occurs, the effect of birefringence on the scattering properties can also be neglected.

Figure 7 shows the phase function P_{11} at $\lambda = 0.55$ μm for 2D plates with an aspect ratio of $L/2a = 0.4$ above [Fig. 7(a)] and below [Fig. 7(b)] the horizon by means of equidistant projection. In this presentation, the diffracted light is excluded so that the reflected and/or the refracted light patterns can be investigated more clearly. The small circle in Fig. 7(a) indicates the incident solar direction. The incident solar zenith angle, θ', is taken

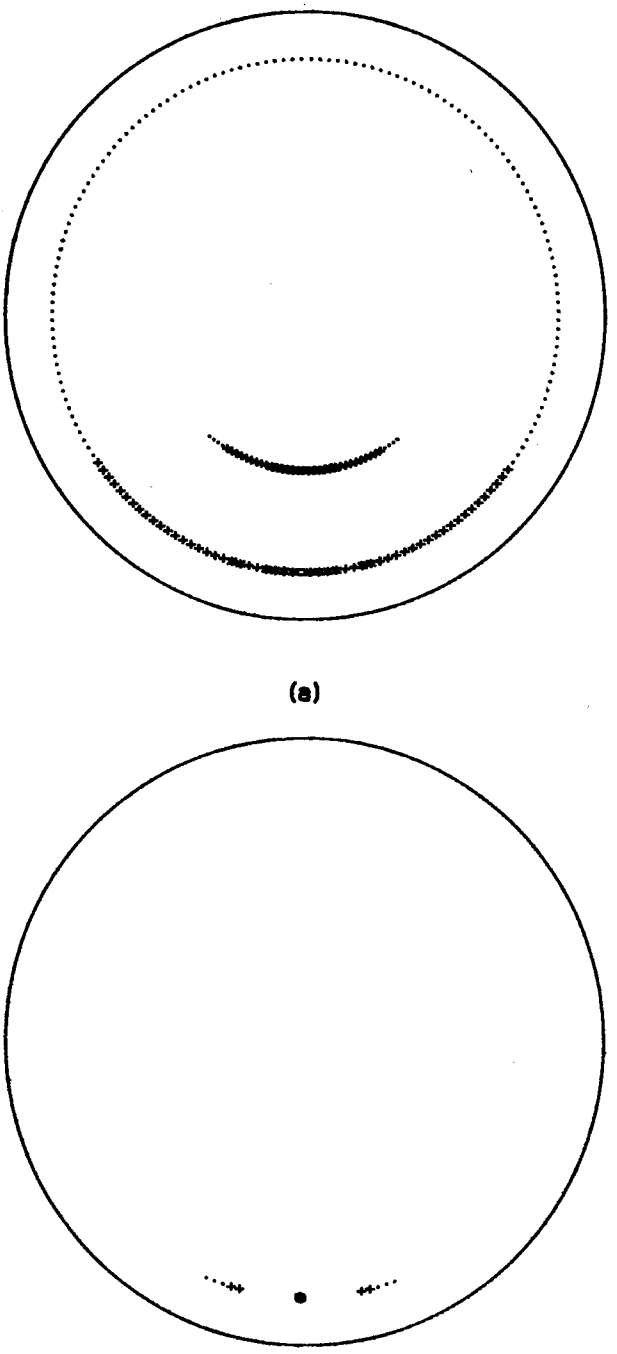

Fig. 9. Same as Fig. 7, except for 2D plates with aspect ratio $L/2a$ of 40/100 (μm/μm) at $\lambda = 10$ μm. The symbols ·, +, *, and ■ denote 0, 1, 2, and 3, respectively, in units of $[\log_{10} P_{11}] + 1$, where [ ] denotes the integral part.

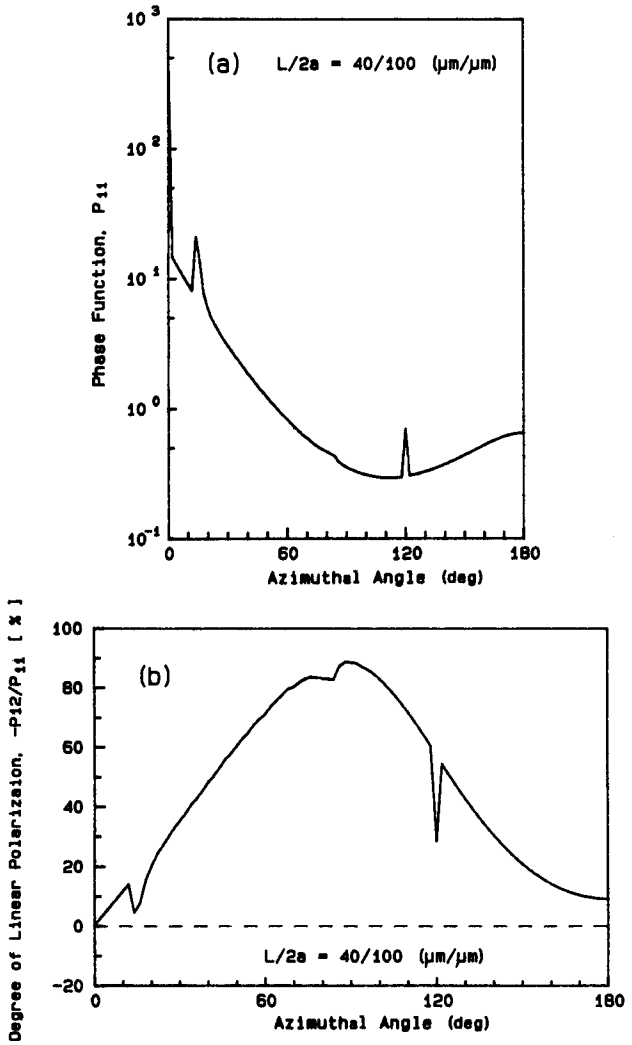

Fig. 10. Same as Fig. 8, except for 2D plates with an aspect ratio $L/2a$ of 40/100 (μm/μm) at $\lambda = 10$ μm.

to be 77°. The scattered light is confined to four latitude circles: the parhelic circle, the circumzenithal arc, the subparhelic circle, and the subcircumzenithal arc. Well-known peaks that are due to the 22° parhelia (sundogs) and to the 120° parhelia on the parhelic circle, as well as peaks that result from the subsun and the subsundogs on the subparhelic circle, can be identified clearly. The halo-phenomenology nomenclature described in this paper follows that of Greenler.[15]

Figure 8 shows the phase function P_{11} corresponding to Fig. 7 and the degree of linear polarization, $-P_{12}/P_{11}$, along the parhelic circle as a function of the azimuthal angle, $\phi - \phi'$. Positive (negative) polarization shows that the electric vector on the scattering plane is smaller (larger) than that perpendicular to this plane. There are two noticeable peaks corresponding to the sundog and to the 120° parhelion [Fig. 8(a)]. Except for negative values of approximately $\phi - \phi' = 30°$ that correspond to the sundog, the degree of linear polarization is positive [Fig. 8(b)]. However, the degree of linear polarization cannot reach +100% as calculated by Lynch,[16] because not only the externally reflected rays ($n = 0$) but also the transmitted rays ($n \geq 1$) can contribute to the parhelic circle outside the sundog.

Figure 9 shows the phase function for 2D plates with an aspect ratio of $L/2a = 40/100$ (μm/μm) at the 10-μm wavelength. As a result of absorption inside the ice crystals, scattered light is contributed mostly from externally reflected rays but also from transmitted rays without internal reflections. As a result, not many optical features can be identified in this case. Because of the difference in real refractive index between the visible and the infrared wavelengths, the position of the circumzenithal arc is different from that produced by visible light. The halos at the 10-μm wavelength in this and in subsequent figures

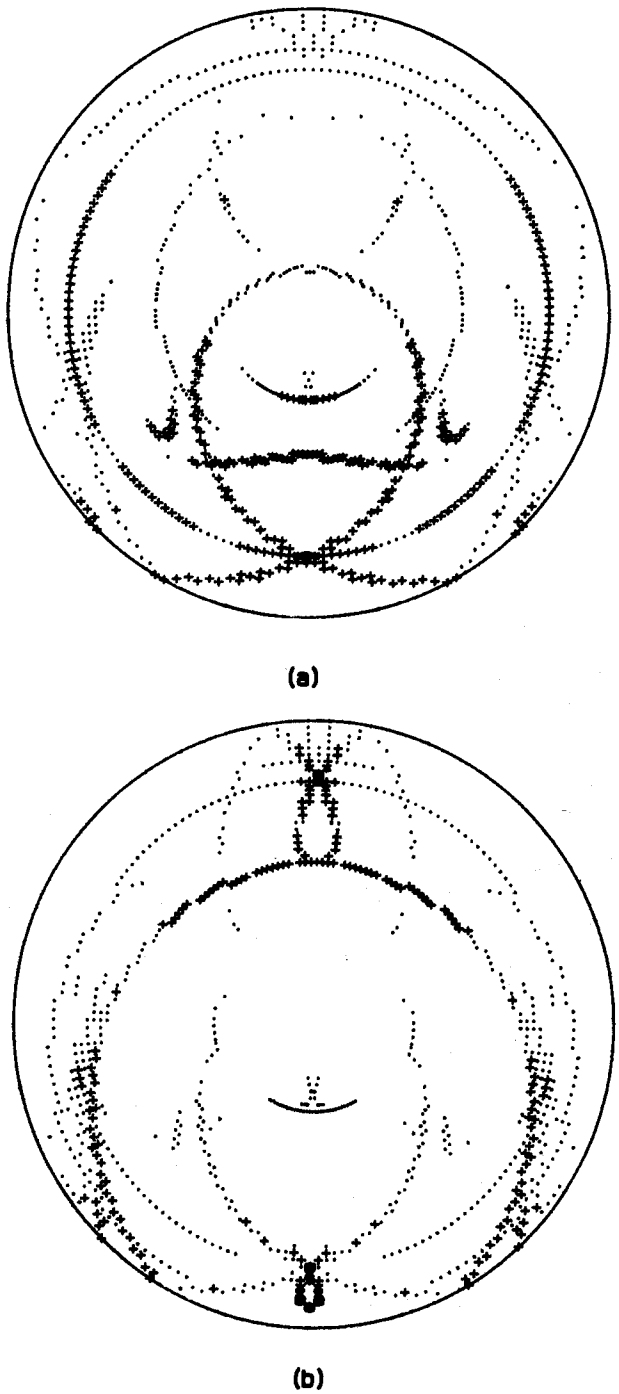

Fig. 11. Same as Fig. 7, except for Parry columns with an aspect ratio $L/2a$ of 2.5 at the solar zenith angle of 73°. The symbols ·, +, *, and ■ denote 0, 1, 2, and 3, respectively, in units of $[\log_{10} P_{11}]$, where [ ] denotes the integral part.

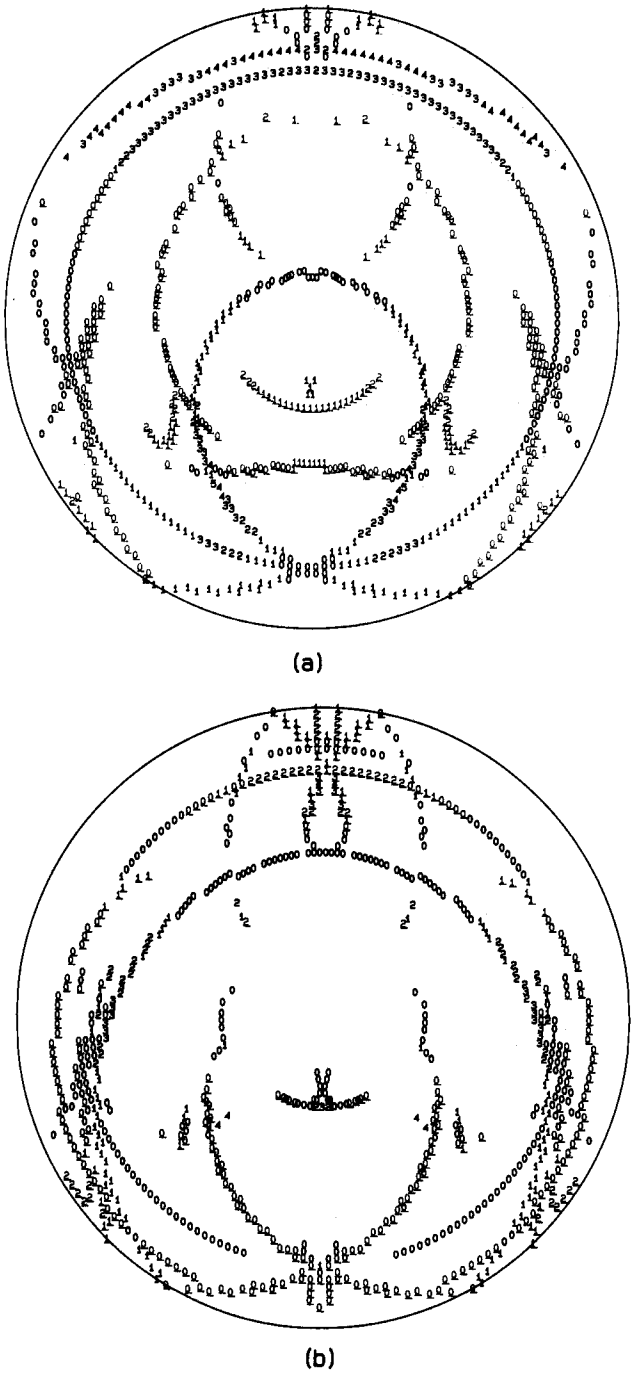

Fig. 12. Degree of linear polarization, $-P_{12}/P_{11}$, for Parry columns (a) above the horizon and (b) below the horizon. The digit 3, for example, denotes a certain value of polarization between +30% and +40%. Digits are underlined when the polarization is negative.

would occur more vaguely than the present computation indicates because of the effect of diffraction, as pointed out by Fraser.[17] However, our intention in Fig. 9 is to compare the 10-μm-wavelength halos with the visible halos for the purpose of checking the computation scheme, not to simulate the 10-μm-wavelength halos.

Figure 10 shows the phase function, P_{11}, corresponding to that in Fig. 9 as well as the degree of linear polarization, $-P_{12}/P_{11}$, along the parhelic circle as a function of the azimuthal angle. The delta function transmission at $\phi - \phi' = 0°$ and the relatively weak peaks resulting from the sundog and the 120° parhelion occur on the parhelic circle produced by externally reflected rays [Fig. 10(a)]. The corresponding degree of linear polarization is positive. As a result of externally reflected rays, the polarization value can reach +90% at $\phi - \phi' = 90°$. Comparing this figure with Fig. 1 of Ref. 2, we can expect that more-positive polarization resulting from the effect of scattering will be produced in this case than in the case of randomly oriented ice crystals.

Figure 11 shows the phase function for Parry columns of $L/2a = 2.5$ at the 0.55-μm wavelength. The incident

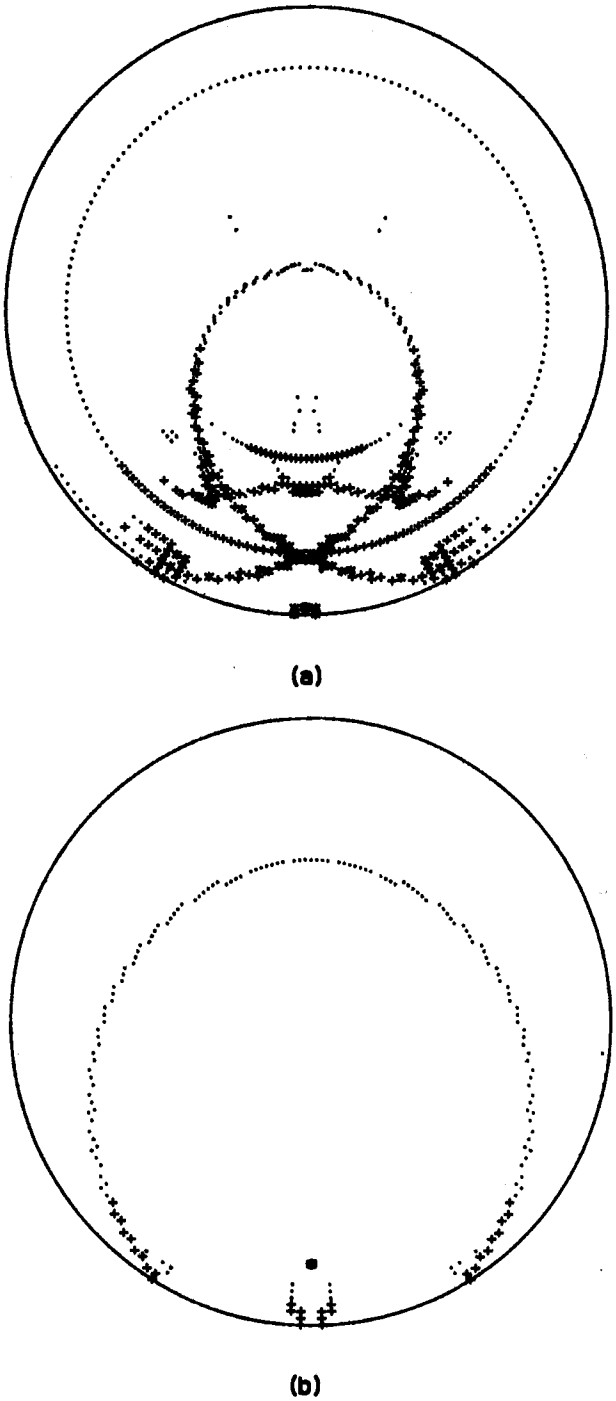

Fig. 13. Same as Fig. 9, except for Parry columns with an aspect ratio $L/2a$ of 120/60 (μm/μm) at $\lambda = 10$ μm. The symbols ·, +, *, and ■ denote 0, 1, 2, and 3, respectively, in units of $[\log_{10} P_{11}] + 1$, where [ ] denotes the integral part.

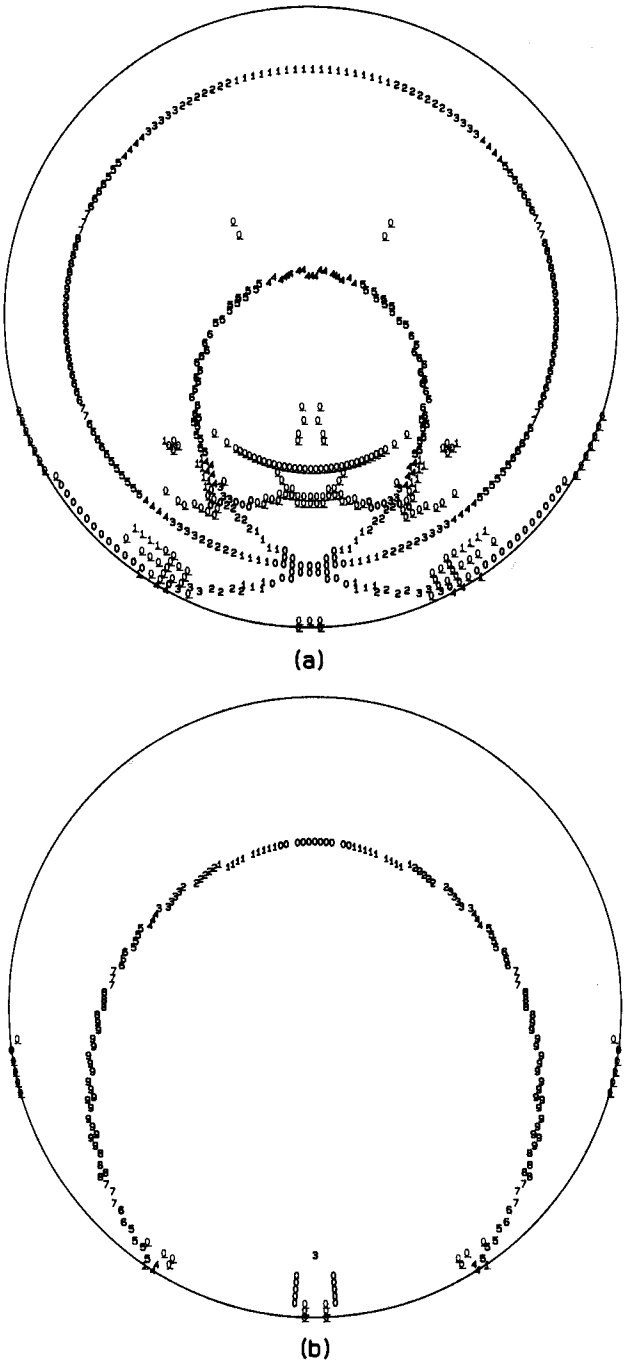

Fig. 14. Same as Fig. 12, except for Parry columns of $L/2a = 120/60$ (μm/μm) at $\lambda = 10$ μm.

solar zenith angle, θ', is 73°. In this figure the upper Parry arc, the lower Parry arc, the parhelic circle, the circumzenithal arc, the heliac arc, the subsun, and the subantihelion are clearly displayed. Figures 11(a) and 11(b) are almost the same as Figs. 3(a) and 3(b), respectively, of Ref. 18, so that the program for the computation of the phase matrix that was developed in this research is consistent with the intensity components.

The degree of linear polarization at $\lambda = 0.55$ μm for Parry columns with aspect ratio of $L/2a = 2.5$ corresponding to P_{11} in Figs. 11(a) and 11(b) is shown in Figs. 12(a) and 12(b), respectively. The numbers in Fig. 12 denote certain values of polarization. For example, number 3 denotes linear polarization between 30 and 40%. The patterns produced by the transmitted rays associated with the Parry arcs and the circumzenithal arc are negatively polarized. According to Greenler,[15] the heliac arc is produced by the externally reflected rays. In light of the small values of linear polarization for the heliac arc displayed in Fig. 12, it appears that the transmitted rays also contribute to its polarization. The polarization pattern shown in Fig. 12(b), if measured from space, can be used for discrimination between ice clouds and snow surfaces in polar regions.

Figure 13 shows the phase function for Parry columns with an aspect ratio of $L/2a = 120/60$ (μm/μm) at the 10-μm wavelength. Because of intense absorption of ice at this wavelength, the phase functions are contributed mostly from the externally reflected and transmitted rays without internal reflections. These patterns should be compared with those illustrated in Fig. 11 for the visible wavelength: the positions of the Parry arcs and of the circumzenithal arc for the 10-μm wavelength differ somewhat from those produced by visible light because of the difference in the real refractive index between the two wavelengths.

Figures 14(a) and 14(b) show the degree of linear polarization, $-P_{12}/P_{11}$, corresponding to P_{11} in Figs. 13(a) and 13(b), respectively. The parhelic circle and the heliac arc, which are produced by the externally reflected rays, are positively polarized. Polarization values close to +100% can be observed on the parhelic circle in Fig. 14(a) and on

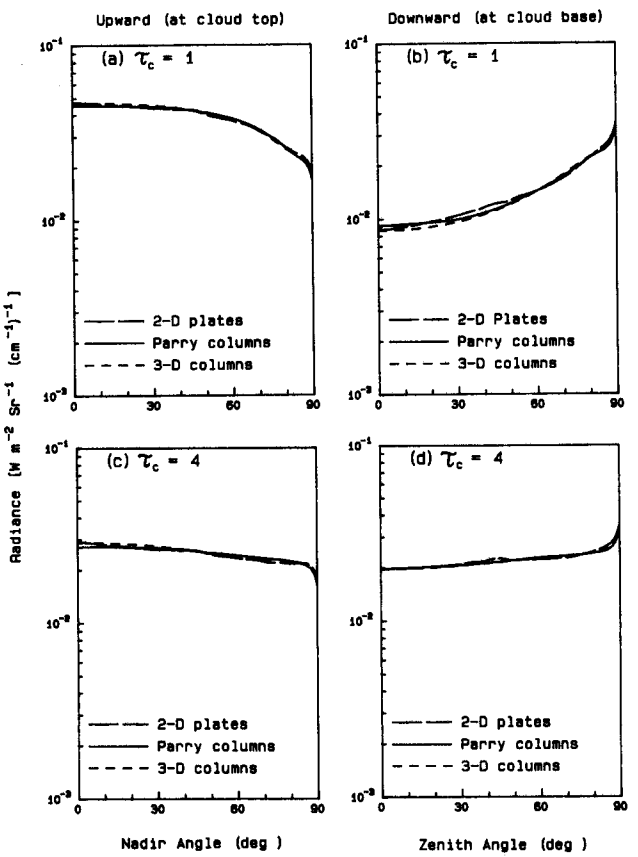

Fig. 15. Radiances as a function of zenith/nadir angles on the boundaries of cirrus clouds in midlatitude winter atmosphere ($T_c = 230$ K and $T_s = 273$ K). (a), (b) Cloud optical depth $\tau_c = 1$; (c), (d) cloud depth $\tau_c = 4$.

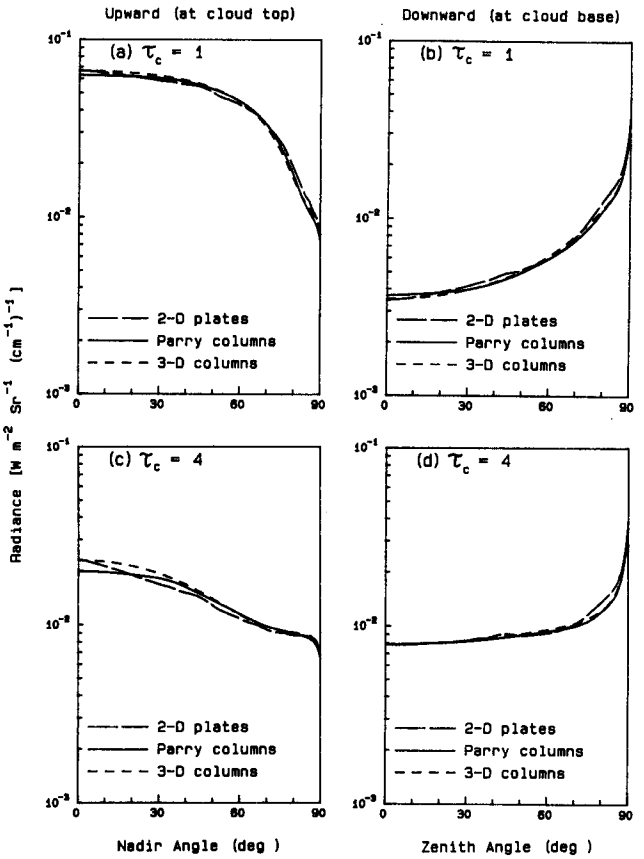

Fig. 16. Same as Fig. 15, except for the tropical atmosphere (T_c = 200 K and T_s = 300 K).

the heliac arc in Fig. 14(b). These values are produced by the externally reflected rays whose incident angle is the Brewster angle. We can also expect more-positive polarization resulting from the effect of scattering in this case than in the case of randomly oriented crystals. Polarization values for the Parry arcs and for the circumzenithal arc (which are produced by the transmitted rays without internal reflections) are slightly negative.

Figure 15 shows the upward radiances emergent from the cloud top and the downward radiances emergent from the cloud base at the 10-μm wavelength. In performing this radiance calculation, we have used the midlatitude winter atmospheric profile (cloud temperature T_c = 230 K and surface temperature T_s = 273 K). The microphysical cloud models used are 2D plates with $L/2a$ = 40/100 (μm/μm) and Parry and 3D (randomly oriented) columns of $L/2a$ = 120/60 (μm/μm). The radiances for horizontally oriented crystals deviate only slightly from those for 3D columns. In both cases, limb darkening and limb brightening appear in the upward and the downward radiances, respectively.

Figure 16 also shows the upward radiances emergent from the cloud top and the downward radiances emergent from the cloud base at the 10-μm wavelength. The tropical atmospheric profile (T_c = 200 K and T_s = 300 K) is used in this computation. The upward radiances near the nadir direction for horizontally oriented crystals are slightly smaller than those for randomly oriented crystals, as shown in Figs. 16(a) and 16(c). However, the radiances for horizontally oriented crystals are, in general, similar to those for randomly oriented crystals. On the basis of the results presented in Figs. 15 and 16, we may conclude that the effect of horizontal orientation may be neglected if the infrared radiances are the only required results.

Figure 17 shows the degree of linear polarization, $-Q/I$, corresponding to Fig. 15, i.e., in the case of midlatitude cirrus. Positive (negative) polarization in the multiple scattering shows that the electric vector on the local meridian plane is smaller (larger) than that perpendicular to this plane. Polarization values for horizontally oriented crystals are greater by an order of magnitude than those for 3D columns, because radiation emitted from horizontally oriented crystals is polarized, whereas radiation emitted from randomly oriented crystals is unpolar-

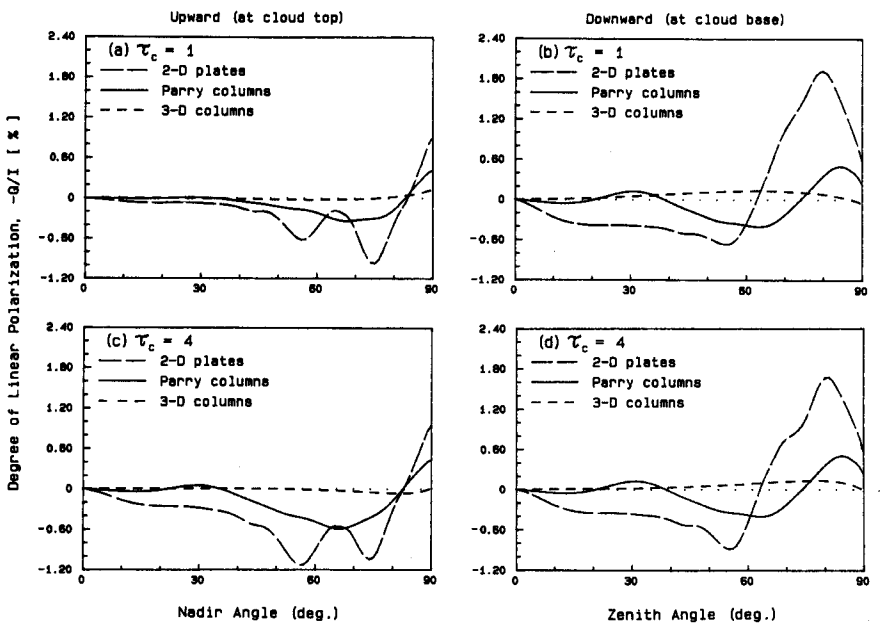

Fig. 17. Degree of linear polarization, $-Q/I$, corresponding to Fig. 15 as a function of zenith/nadir angles on the boundaries of cirrus clouds in the midlatitude winter atmosphere: (a), (b) cloud optical depth τ_c = 1; (c), (d) cloud depth τ_c = 4.

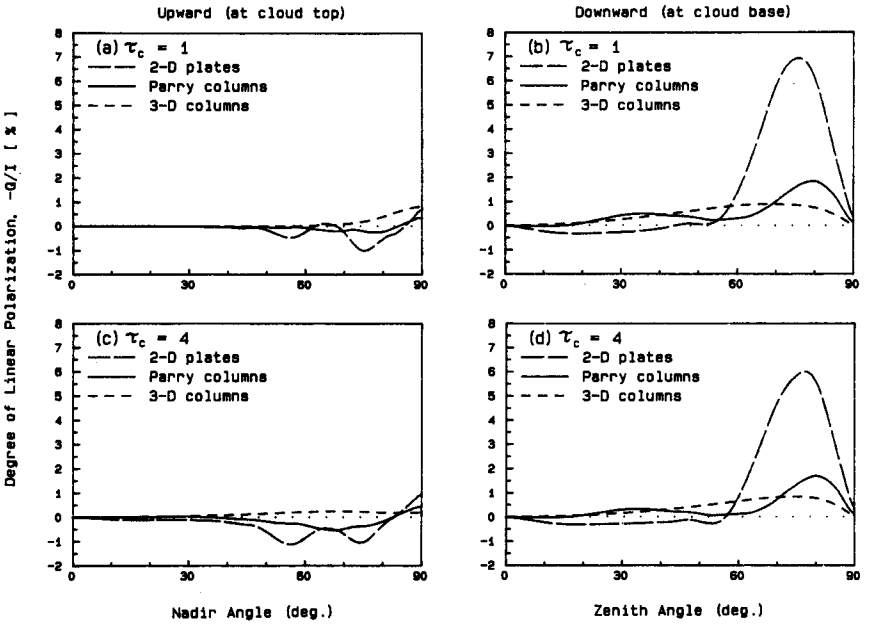

Fig. 18. Same as Fig. 17, except for the tropical atmosphere.

ized. The patterns of the linear polarization in this figure resemble those of the linear polarization, $-Q_e$, emitted from horizontally oriented crystals as shown in Fig. 2. However, we can see local maximum values at $\theta = 65°$ in Figs. 17(a) and 17(c) and maximum values at $\theta = 77°$ in Figs. 17(b) and 17(d), which are produced by the effect of scattering in the case of 2D plates. These maxima can be interpreted as follows: In the case of 2D plates, scattered light is confined to four latitude circles and is contributed mostly from the externally reflected rays. Diffuse reflections are produced by reflections at the basal plane of 2D plates. For the reflected light at a zenith angle θ the corresponding incident angle is θ. As a result, at a certain zenith angle the maximum value of positive polarization appears, as shown in Figs. 17(b) and 17(d). Diffuse transmissions are produced by reflections at the six prism planes of 2D plates. For scattered light at a nadir angle θ, the corresponding maximum incident angle is $\pi/2 - \theta$. For this reason, the local maximum of polarization appears at a different nadir angle, as shown in Figs. 17(a) and 17(c). The effect of scattering in upward radiances is weaker than that in downward radiances at limb directions. As a result, the (local) maximum values shown in Figs. 17(a) and 17(c) are smaller than those shown in Figs. 17(b) and 17(d).

The magnitudes of negative upward polarization shown in Figs. 17(a) and 17(c) become larger when optical depth increases, because negatively polarized radiation emitted from horizontally oriented crystals is more predominant than unpolarized radiation emitted from the ground. On the other hand, downward polarization remains unchanged when optical depth increases, as shown in Figs. 17(b) and 17(d), because polarization from both cloud reflection and cloud emission is weakly dependent on optical depth.

Figure 18 shows the degree of linear polarization for tropical cirrus corresponding to Fig. 16. Upward polarization values in Figs. 18(a) and 18(c) are close to those for midlatitude cirrus shown in Figs. 17(a) and 17(c). This is because unpolarized radiation emitted from the ground at small nadir angles and cloud emission at other nadir angles contribute to the upward radiation. Downward polarization values in Figs. 18(b) and 18(d) are different from those for midlatitude cirrus in Figs. 17(b) and 17(d). Positive polarization values are larger and reach +7% at the zenith angle of 77°, because the cloud temperature, T_c, is much colder than the surface temperature, T_s, for tropical cirrus. Therefore positively polarized cloud reflection relative to weakly polarized cloud emission is more dominant for tropical cirrus than for midlatitude cirrus. Small ice crystals with sizes of less than ~40 μm may exist in both tropical and midlatitude cirrus clouds, as is discussed in Ref. 19. These small ice crystals tend to orient randomly in space[17] and may reduce the percentage of linear polarization presented in Figs. 17 and 18. The degree of reduction would depend on the number density of small ice crystals that are present in the cloud.

5. CONCLUSIONS

Extending our previous research on the evaluation of radiance and linear-polarization patterns for randomly oriented hexagonal ice crystals, we have developed a theory to compute radiances and linear-polarization distributions for horizontally oriented ice crystals at thermal infrared wavelengths. A numerical program for computing the phase matrix elements for horizontally oriented crystals was developed in the present study on the basis of the procedure outlined in Ref. 4. For the first time to our knowledge, we derived the symmetry relations of the phase matrix and the linear polarization of thermal emission for horizontally oriented crystals. A 2 × 2 phase matrix in reference to the local meridian plane is sufficient for computing linear polarization for infrared radiation in multiple-scattering processes.

The phase matrices for horizontally oriented crystals were calculated at the 0.55- and 10-μm wavelengths. We find that positive polarization values of the parhelic

circle at the visible wavelength cannot reach +100%, a finding that differs from the results that we obtained in our previous study. Computations of infrared radiative transfer are carried out by means of the adding method with the use of the midlatitude-winter and tropical-atmospheric profiles. If one is interested only in infrared radiances, it is sufficient to use the randomly oriented crystal model in the computation. In this case, the effect of horizontal orientation can be neglected. However, the effect of crystal orientation is important for the generation of linear polarization at infrared wavelengths. The degree of linear polarization in the case of randomly oriented crystals is zero or slightly positive, with values of only as much as +1%. In the case of horizontally oriented crystals, linear polarization is negative, with values of approximately −1% at the cloud top, whereas it can have a maximum value of +7% at the cloud base.

In view of these findings, it appears that it is possible to infer the orientation properties of ice crystals in cirrus clouds by measuring infrared polarization from the ground or from aircraft above cirrus clouds.

ACKNOWLEDGMENTS

This research has been supported by the U.S. Office of Naval Technology through the U.S. Naval Air Warfare Center, Aircraft Division, Warminster, Pennsylvania, under contract N62269-89-C-0561, by the U.S. Air Force Office of Scientific Research under grant AFOSR-91-0039 and in part by the National Science Foundation and by grant ATM 90-24217. Some of the computations contained in this research have been carried out on the San Diego supercomputer, Cray Y-MP 8/864. We thank M. Hess for helpful comments on this paper.

REFERENCES

1. K. N. Liou, Y. Takano, S. C. Ou, A. J. Heymsfield, and W. Kreiss, "Infrared transmission through cirrus clouds: a radiative model for target detection," Appl. Opt. **29,** 1886–1896 (1990).
2. Y. Takano and K. N. Liou, "Infrared polarization signature from cirrus clouds," Appl. Opt. **31,** 1916–1919 (1992).
3. L. Thomas, J. C. Cartwright, and D. P. Wareing, "Lidar observations of the horizontal orientation of ice crystals in cirrus clouds," Tellus **42B,** 211–216 (1990).
4. Y. Takano and K. N. Liou, "Solar radiative transfer in cirrus clouds. Part I: single-scattering and optical properties of hexagonal ice crystals," J. Atmos. Sci. **46,** 3–19 (1989).
5. Y. Takano and K. N. Liou, "Solar radiative transfer in cirrus clouds. Part II: theory and computation of multiple scattering in an anisotropic medium," J. Atmos. Sci. **46,** 20–36 (1989).
6. K. N. Liou, *An Introduction to Atmospheric Radiation* (Academic, New York, 1980), Chap. 6, p. 222.
7. S. Warren, "Optical constants of ice from the ultraviolet to the microwave," Appl. Opt. **23,** 1206–1225 (1984).
8. P. Minnis, K. N. Liou, and Y. Takano, "Inference of cirrus cloud properties using satellite-observed visible and infrared radiances. Part I: parameterization of radiance fields," J. Atmos. Sci. (to be published).
9. Y. Takano and K. Jayaweera, "Scattering phase matrix for hexagonal ice crystals computed from ray optics," Appl. Opt. **24,** 3254–3263 (1985).
10. H. C. van de Hulst, *Light Scattering by Small Particles* (Wiley, New York, 1957), Chap. 5, p. 44.
11. Y. Takano and S. Asano, "Fraunhofer diffraction by ice crystals suspended in the atmosphere," J. Meteorol. Soc. Jpn. **61,** 289–300 (1983).
12. J. W. Hovenier, "Symmetry relationships for scattering of polarized light in a slab of randomly oriented particles," J. Atmos. Sci. **26,** 488–499 (1969).
13. H. C. van de Hulst, *Multiple Light Scattering* (Academic, New York, 1980), Chap. 15, p. 505.
14. Q. Cai and K. N. Liou, "Polarized light scattering by hexagonal ice crystals: theory," Appl. Opt. **21,** 3569–3580 (1982).
15. R. G. Greenler, *Rainbows, Halos, and Glories* (Cambridge U. Press, New York, 1980), Chap. 3, p. 92.
16. D. K. Lynch, "Polarization models of halo phenomena. I. The parhelic circle," J. Opt. Soc. Am. **69,** 1100–1103 (1979).
17. A. B. Fraser, "What size of ice crystals causes the halos?" J. Opt. Soc. Am. **69,** 1112–1118 (1979).
18. Y. Takano and K. N. Liou, "Halo phenomena modified by multiple scattering," J. Opt. Soc. Am. A **7,** 885–889 (1990).
19. Y. Takano, K. N. Liou, and P. Minnis, "The effects of small ice crystals on cirrus infrared radiative properties," J. Atmos. Sci. **49,** 1487–1493 (1992).